Received 3 September 2020; revised 7 October 2020; accepted 7 October 2020. Date of publication 12 October 2020; date of current version 5 November 2020.

Digital Object Identifier 10.1109/OJAP.2020.3030091

Error Analysis of Higher Order Bivariate Lagrange and Triangular Interpolations in Electromagnetics

WEN LUO [1,2], JINBO LIU [1,2], ZENGRUI LI [1,2] (Member, IEEE), AND JIMING SONG [3] (Fellow, IEEE)

[1]State Key Laboratory of Media Convergence and Communication, Communication University of China, Beijing 100024, China

[2]School of Information and Communication Engineering, Communication University of China, Beijing 100024, China

[3]Department of Electrical and Computer Engineering, Iowa State University, Ames, IA 50011, USA

CORRESPONDING AUTHORS: J. LIU AND J. SONG (e-mail: liuj@cuc.edu.cn; jisong@iastate.edu)

This work was supported in part by the National Natural Science Foundation of China under Grant 61971384, Grant 61701447, and Grant 62071436; in part by the Fundamental Research Funds for the Central Universities under Grant CUC2019B068, Grant CUC19ZD001, and Grant CUC200D054; and in part by the Key Laboratory of All Optical Network and Advanced Telecommunication Network, Ministry of Education, Beijing Jiaotong University under Grant ZG19002.

ABSTRACT The interpolation errors of the higher order bivariate Lagrange polynomial interpolation based on the rectangular, right and equilateral triangular interpolations are measured by using the maximum and root-mean-square (RMS) errors. The error distributions of above three kinds of interpolations are analyzed to find the regions having the smallest interpolation error. Both analytical and numerical results show that the right triangular interpolation is the most efficient interpolation method. Although both the maximum and RMS errors of the right triangular interpolation are larger than that of the rectangular interpolation, the number of data points used in the triangular interpolation is up to 50% less than that used in the rectangular one. On the other hand, the equilateral triangular interpolation using the regions inside a big triangle as interpolation area is proved to be the most accurate interpolation method. The interpolation errors of the equilateral triangular are almost half of that of the rectangular interpolation. In addition, the right triangular, equilateral triangular and rectangular interpolations for the third and fourth orders are applied to accelerate the calculation of doubly periodic Green's function (PGF).

INDEX TERMS Doubly periodic Green's function (PGF), Lagrange polynomial interpolation, maximum error, plane waves, root-mean-square (RMS) error, triangular interpolations.

I. INTRODUCTION

INTERPOLATION has been widely used in many areas of computational electromagnetics (CEM) to save the CPU time, e.g., the moment method, the finite element method (FEM), and so on [1]–[5]. Accurate and efficient evaluation of free-space periodic Green's functions (PGF) takes an important role in CEM [6], [7]. The PGF with two-dimensional (2-D) lattices is in the form of double infinite spectral and spatial summations, which is usually slowly convergent [8], [9]. For the doubly PGF, it is not efficient to direct calculate all observation and source points, which poses a challenging problem drawing great interests from researchers [10], [11]. The Ewald and the Kummer's methods are two robust and efficient methods to accelerate the evaluation of PGF, which are still time consuming however [12]. Pre-calculated PGFs are applied to evaluate the PGF using the interpolation method within a certainly accuracy to reduce the CPU time [12]–[14].

There are several approaches for interpolations such as bivariate Lagrange polynomials and approximate prolate spheroidal (APS) interpolations [3], [15], [16]. The commonly used interpolation technique is a product of the rectangular Lagrange interpolations, where $(p+1)^2$ points will be used for the p'th order interpolation in 2-D. However, in FEM, about only half of those points are applied for interpolations of all points inside a big triangular area, which is not the most optimized interpolated region [4], [17]. Choosing the center of a triangle as the interpolation area can reduce the interpolation error. In [14], the region with the smallest interpolation error inside a big triangle is chosen to

reduce the interpolation error for the first and second order interpolations.

It is quite clear that the higher degree of interpolation polynomials, the more reduction in the number of data points used in the triangular interpolation over the rectangular interpolation. This article focuses on choosing the regions with the smallest error of the higher orders triangular interpolations, while the maximum and RMS errors are considered as the interpolation error measurements. In addition, the asymptotic expressions of maximum and RMS errors for one-dimensional (1-D) and 2-D interpolations are derived. The organization of this article is as follows. In Section II, the asymptotic forms of the maximum and RMS errors for 1-D are derived. How to select the 2-D interpolation areas for higher order interpolations is presented in Section III. Section IV provides the expression of doubly PGF using Ewald method, the regularized doubly PGF which has removed the singularity to smooth the function to be interpolated, and the numerical results for the application of the doubly PGF. Some conclusions about the triangular interpolations are given in Section V. Finally, some details of the derivations are shown in Appendix.

II. INTERPOLATION ERROR OF PLANE WAVE IN 1-D

The plane wave is applied to study the interpolation error in 1-D, which is simply expressed as $J(x) = e^{-jkx}$. The Lagrange interpolation polynomial is given as (13) in Appendix [17], [18]. The error definition and asymptotic forms of maximum and RMS errors for the first and second order interpolations are presented in [14]. The nearest $p+1$ points are used to interpolate a function at a given point with the p'th order polynomial. The asymptotic form of maximum error is derived as

$$R_p^{\text{Max}} = (kh/2)^{p+1}(2l-1)!!/(2l)!!,\ l = \text{int}\big[(p+1)/2\big], \quad (1)$$

for uniform sampling with a distance of h, where "int" is a function to pick up the integer part. For even orders $p = 2l$, the asymptotic form of RMS error is calculated by

$$R_p^{\text{RMS}} = \frac{(kh/2)^{p+1}}{(p+1)!}\sqrt{\int_0^1 dx\, x^2 \prod_{i=1}^{l}\left(x^2-4i^2\right)^2} \quad (2a)$$

and for odd orders $p = 2l-1$,

$$R_p^{\text{RMS}} = \frac{(kh/2)^{p+1}}{(p+1)!}\sqrt{\int_0^1 dx\,(x-2l)^2 x^2 \prod_{i=1}^{l-1}\left(x^2-4i^2\right)^2} \quad (2b)$$

From the asymptotic expressions, the maximum and RMS errors are directly proportional to the $(p+1)$'th power of kh. The analytical expressions for the maximum and RMS errors are listed in Tables 1 and 2, respectively. Table 3 gives the asymptotic forms of the errors and the ratios between the asymptotic maximum and RMS errors. The ratio between the maximum and RMS errors approaches to $\sqrt{2}$ as the order of interpolations increases. Figures 1 (a) and (b) plot the analytical (Ana) and asymptotic (Asm) maximum and RMS errors over different numbers of samples per wavelength, respectively. It is observed that the asymptotical results agree well with the analytical ones.

TABLE 1. 1-D analytical maximum interpolation error for plane wave.

Order p	R_p^{Max}
0	$2\sin x$
1	$2\sin^2 x$
2	$2\sin^3 x\sqrt{3\cos^2 x+1}$
3	$2\sin^4 x\left(2\cos^2 x+1\right)$
4	$2\sin^5 x\sqrt{15\cos^6 x+15\cos^4 x+5\cos^2 x+1}$

where $x = kh/4$.

TABLE 2. 1-D analytical RMS interpolation error for plane wave.

Order p	R_p^{RMS}
0	$\sqrt{2-\sin(2x)/x}$
1	$\sqrt{\left[-3+20x^2+\left(3+4x^2\right)\cos\left(4x\right)\right]/\left(12x^2\right)}$
2	$\sqrt{1-\frac{\left(1+2x^2\right)\sin^3(2x)}{8x^3}-\frac{17}{120}\sin^4(2x)}$

where $x = kh/4$. The expressions for higher orders are too long and not listed here to save the space.

TABLE 3. 1-D interpolation error for plane wave in asymptotic form.

Order p	R_p^{Max}	R_p^{RMS}	$R_p^{\text{Max}}/R_p^{\text{RMS}}$
0	$\frac{kh}{2}$	$\frac{kh}{2\sqrt{3}}$	1.732
1	$\frac{1}{2}\left(\frac{kh}{2}\right)^2$	$\sqrt{\frac{2}{15}}\left(\frac{kh}{2}\right)^2$	1.369
2	$\frac{1}{2}\left(\frac{kh}{2}\right)^3$	$\frac{\sqrt{407}}{6\sqrt{105}}\left(\frac{kh}{2}\right)^3$	1.524
3	$\frac{3}{8}\left(\frac{kh}{2}\right)^4$	$\frac{\sqrt{206}}{9\sqrt{35}}\left(\frac{kh}{2}\right)^4$	1.391
4	$\frac{3}{8}\left(\frac{kh}{2}\right)^5$	$\frac{\sqrt{128123}}{72\sqrt{385}}\left(\frac{kh}{2}\right)^5$	1.480

III. INTERPOLATION ERROR OF PLANE WAVES IN 2-D

In 2-D interpolation, the plane waves are simply expressed as $J(x, y, \alpha) = e^{-jk(x\cos\alpha+y\sin\alpha)}$, where α is the propagation direction. Although the coefficients of interpolation errors for arbitrarily complex cases are different, the interpolation errors majorly depend on the order of interpolations. The coefficients of the errors are related to the specific function to be interpolated. The definitions of relative, maximum and RMS interpolation errors for different angles and locations are given in [14]. For 2-D interpolation, both the maximum

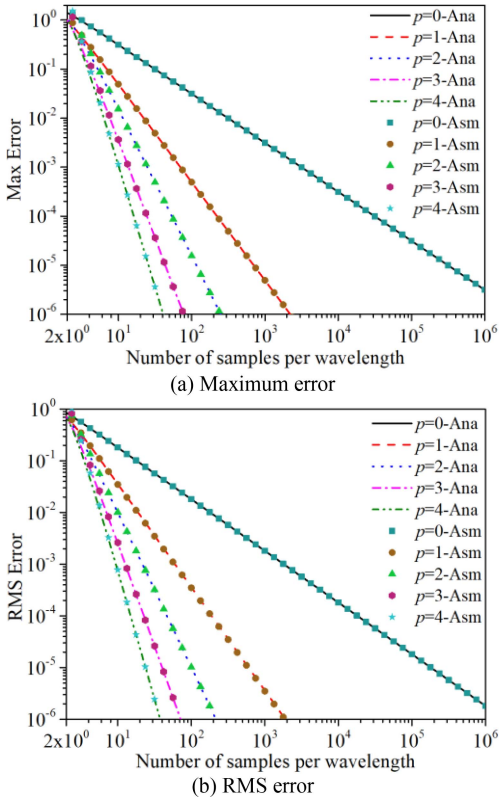

FIGURE 1. Maximum and RMS errors of the 1-D Lagrange interpolations from order 0 to 4. "Ana" stands for the analytical results, and "Asm" for the asymptotic results.

and RMS errors are functions of locations and propagation directions.

The asymptotic forms of maximum and RMS errors are derived. For the rectangular Lagrange interpolation, the expression of the maximum error is

$$R_{p,q}^{\mathrm{Max}} = \left|J(x,y,\alpha) - L_p(x)L_q(y)\right|_{\mathrm{Max}} \tag{3}$$

where p and q are the interpolations orders along x and y, respectively. In the Appendix, the asymptotic form is derived as

$$R_{p,q}^{\mathrm{Max}} \le R_p^{\mathrm{Max}}(kh|\cos\alpha|) + R_q^{\mathrm{Max}}(kh|\sin\alpha|) \tag{4}$$

where R_p^{Max} is the maximum error for the p'th order interpolation as shown in (1) by replacing kh with $kh|\cos\alpha|$ or $kh|\sin\alpha|$. If $p = q$, the asymptotic form of maximum error is simplified as

$$R_{p,p}^{\mathrm{Max}}(\alpha) \le \frac{\left(2\left[(p+1)/2\right]-1\right)!!}{\left(2\left[(p+1)/2\right]\right)!!}\left(\frac{kh}{2}\right)^{p+1} Q(\alpha) \tag{5}$$

where $Q(\alpha) = |\cos\alpha|^{p+1} + |\sin\alpha|^{p+1}$. The asymptotic RMS error for the rectangular Lagrange interpolation is derived as:

$$R_{p,p}^{\mathrm{RMS}} \approx R_p^{\mathrm{RMS}}(kh) \times \begin{cases} \cos^{(p+1)}\alpha + \sin^{(p+1)}\alpha & p \text{ is odd} \\ \sqrt{\cos^{2(p+1)}\alpha + \sin^{2(p+1)}\alpha} & p \text{ is even} \end{cases} \tag{6}$$

TABLE 4. Number of data points used in the rectangular (□), right triangular (◿) and equilateral triangular (△) interpolations.

Order p	□	◿	△
0	1	1	1
1	4	3	3
2	9	6	6
3	16	10	10
4	25	15	15

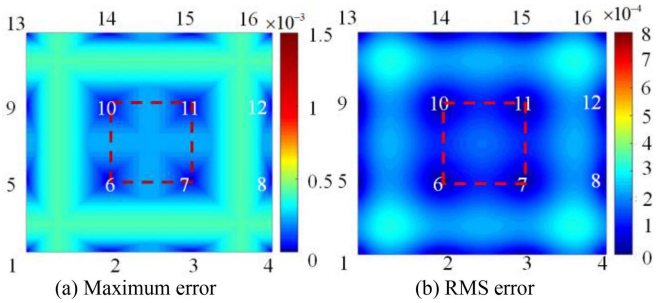

FIGURE 2. $p = 3$, the error distributions of rectangular interpolation, where the rectangle at the center is the interpolation area, $\lambda/h = 20$.

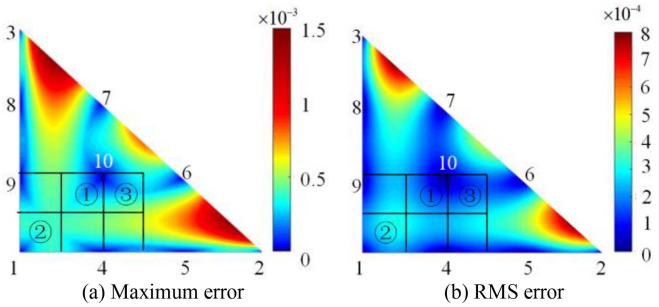

FIGURE 3. $p = 3$, the error distributions of right triangular interpolation, where Area 1 is the interpolation area, $\lambda/h = 20$.

where R_p^{RMS} is the RMS error for the p'th order interpolation as shown in (2a) and (2b).

Table 4 lists the numbers of data points used in the rectangular, right triangular and equilateral triangular interpolations. It is found that the samples of the right triangular grid are the same as the rectangular grid, while the data points used for interpolations are up to 50% less than the rectangular interpolation at the same order. The mesh size of equilateral triangular interpolation is the same as the rectangular grid, that is to say, the distance between the two adjacent data points along y-direction is shorter than the rectangular grid, while that along x-direction is the same as the rectangular grid. Thus, the number of samples along y-direction is more than x-direction. As shown in [14], the distance of two adjacent points of the equilateral triangular is $\sqrt{3}/2$ of the rectangular grid along y-direction, while the triangular interpolations use $p(p+1)/2$ data points less at the same order.

A. 3RD ORDER INTERPOLATION

For the third order interpolation, the numbers of data points for the rectangular and triangular interpolations are 16 and

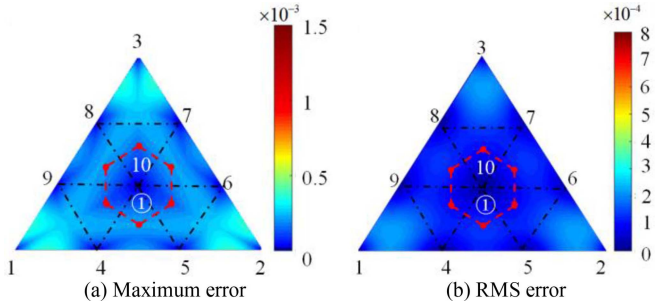

(a) Maximum error (b) RMS error

FIGURE 4. $p = 3$, the error distributions of equilateral triangular interpolation, where the regular hexagon at the center is the interpolation area, $\lambda/h = 20$.

TABLE 5. Numerical maximum and RMS errors for areas 1, 2, 3 shown in Fig. 3 (a) and (b), $\lambda/h = 20$.

Area	Max errors	RMS errors
①	0.000469	0.000197
②	0.000426	0.000247
③	0.000583	0.000175

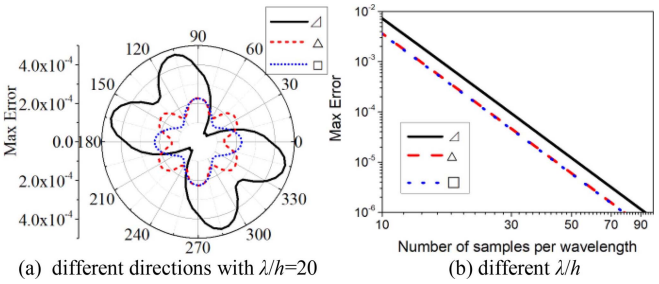

(a) different directions with λ/h=20 (b) different λ/h

FIGURE 5. $p = 3$, the maximum errors of the right triangular (◿), equilateral triangular (△) and rectangular (□) interpolations.

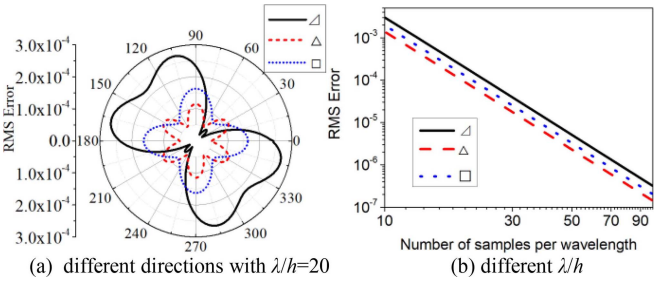

(a) different directions with λ/h=20 (b) different λ/h

FIGURE 6. $p = 3$, the RMS errors of the right triangular (◿), equilateral triangular (△) and rectangular (□) interpolations.

10, respectively. Figures 2, 3 and 4 show the numerical maximum and RMS error distributions for rectangular, right and equilateral triangular interpolations for different angles, respectively. The right triangular interpolation has the largest interpolation errors, while both the largest maximum and RMS errors appear between points 3 and 7 or 2 and 6. The equilateral triangular interpolation has the smallest maximum and RMS errors. Meanwhile, the largest maximum and RMS errors of the equilateral triangular interpolation are almost half of the rectangular interpolation. The equilateral triangular interpolation has the smallest maximum and RMS errors. Through choosing the small interior rectangle with the smallest interpolation errors, the interpolation errors of right triangular interpolation are closer to the rectangular one.

From Fig. 2 (a) and (b), it is easy to observe that the optimal interpolation area is a rectangle formed by points 6, 7, 10, and 11. The region with the smallest error for the equilateral triangular interpolation is the overlap of a regular hexagon at the center with three small triangles [(4, 10, 9), (6, 10, 5), and (7, 10, 8)], as shown in Fig. 4 (a) and (b). To reduce the interpolation error of the right triangular interpolation, the numerical interpolation errors of Area 1, Area 2 and Area 3 are analyzed to find the area with the lowest interpolation error, as shown in Fig. 3 (a) and (b). Table 5 lists the numerical maximum and RMS errors of these areas. It is found that Area 2 has the lowest maximum error and the largest RMS error. On the contrary, Area 3 has the largest maximum error and the lowest RMS error. Both the maximum and RMS errors in Area 1 are the middle ones among these three areas. Thus, the interpolation error distribution in Area 1 is more uniform than other areas. The Area 1 is chosen as the interpolation area for the right triangular interpolation of third order.

Figures 5 and 6 plot the numerical maximum and RMS errors of the right triangular, equilateral triangular and rectangular interpolations over different propagation directions and different numbers of samples per wavelength. It is found that the maximum error of the right triangular interpolation is 107% more than the rectangular interpolation, while it only uses 10 data points for interpolation. For the same maximum error, the equilateral triangular interpolation needs the same number of samples per wavelength as the rectangular interpolation, which is less than that of the right triangular one.

From the above discussion, we find how to look for the data points used in the third order interpolation for a given point. For the rectangular interpolation, find four nearest points, i.e., points 6, 7, 11, and 10 in Fig. 2. Then add next 12 nearest points to be used in the interpolation. For the right triangular interpolations, to interpolate any point inside Region ① in Fig. 3, firstly, three nearest data points are found to form a small right triangle, i.e., points 4, 10, and 9. Secondly, next three nearest points are added, i.e., points 1, 5, and 8, to form a medium right triangle. Finally, extend four more data points along the hypotenuse of the right triangle to form a big one. For the equilateral triangular interpolation, to interpolate any point inside Region ① for example, find the nearest data point, i.e., point 10, then add six nearest points from the point, i.e., points 4, 5, 6, 7, 8, and 9. After that a regular hexagon is obtained, then extend another three points, i.e., points 1, 2, 3, to form a big equilateral triangle.

B. 4TH ORDER INTERPOLATION

For the fourth order interpolation, the triangular interpolation uses 10 data points less than the rectangular interpolation,

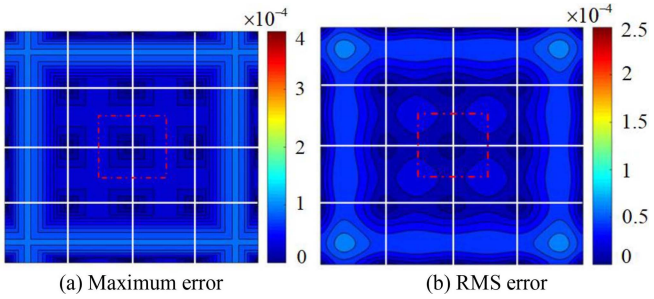

FIGURE 7. $p = 4$, the error distributions of rectangular interpolation, the rectangle formed by red dashed lines at the center is the interpolation area, $\lambda/h = 20$.

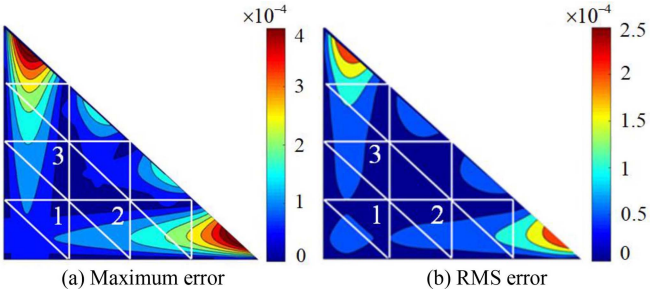

FIGURE 8. $p = 4$, the error distributions of right triangular interpolation, $\lambda/h = 20$. The error distributions inside the small triangle formed by points 1, 2, and 3 are further analyzed in Fig. 10.

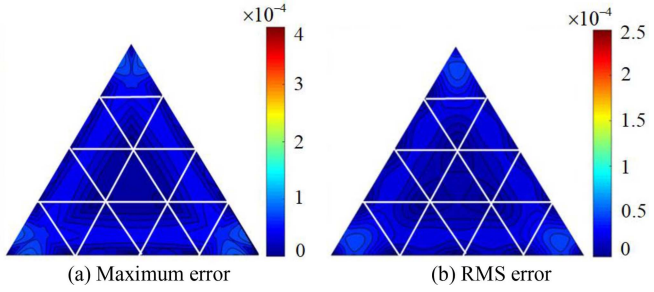

FIGURE 9. $p = 4$, the error distributions of equilateral triangular interpolation, while the equilateral triangle at the center is the interpolation area, $\lambda/h = 20$.

as shown in Table 4. Figures 7, 8 and 9 show the numerical maximum and RMS error distributions of the right triangular, equilateral triangular and rectangular interpolations for different propagation directions, respectively. For the right triangular interpolation, as plotted in Fig. 8, the small right triangle at the center is divided into three parts (one rectangle and two small right triangles, as shown in Fig. 10) to look for the region with the smallest interpolation error, similar to the discussion for the first order in [14]. The error distributions of the small triangle are shown in Fig. 10 (a) and (b). The numerical results of Regions 1 and 2 are listed in Table 6. It is obvious that the maximum error of Region ② is larger than that of Region ①, while the RMS errors of two regions are quite close. In addition, in order to ensure the interpolation areas for high-order interpolations are similar to the low-order interpolations, Region ① is chosen as the interpolation area for the fourth order right triangular interpolation.

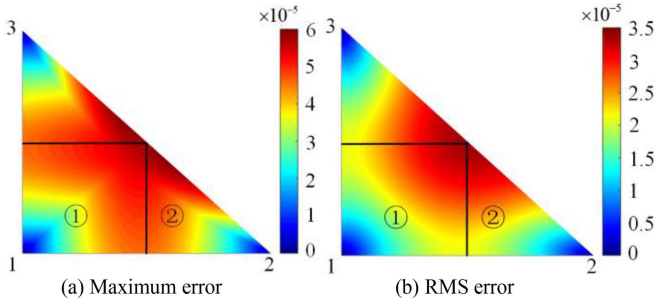

FIGURE 10. $p = 4$, the error distributions of small right triangle at the center of big right triangle as shown in Fig. (8), which is divided into three parts, $\lambda/h = 20$.

TABLE 6. Numerical maximum and RMS errors for areas 1 and 2 shown in Fig. 10 (a) and (b), $\lambda/h = 20$.

Area	Max errors	RMS errors
①	5.75e-05	2.31e-05
②	5.94e-05	2.29e-05
small triangle	5.94e-05	2.30e-05

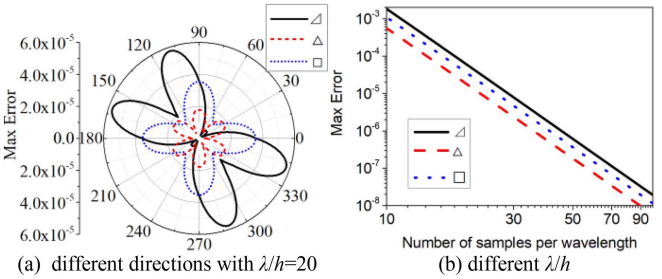

FIGURE 11. $p = 4$, the maximum errors of the right triangular (◿), equilateral triangular (△) and rectangular (□) interpolations.

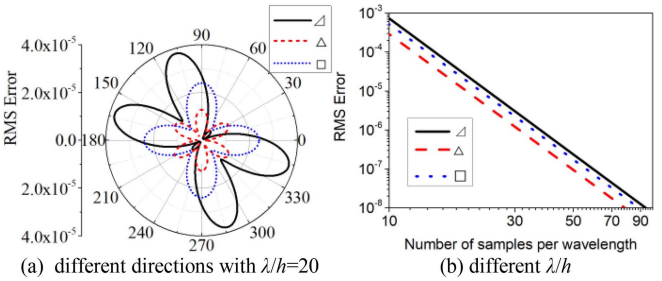

FIGURE 12. $p = 4$, the RMS errors of the right triangular (◿), equilateral triangular (△) and rectangular (□) interpolations.

Figure 11 and 12 plot the numerical maximum and RMS errors of the right triangular, equilateral triangular and rectangular interpolations over different propagation directions and different number of samples per wavelength for the fourth order interpolation, respectively. As is shown, the maximum error of the right triangular interpolation is 62.4% larger than that of the rectangular interpolation. The maximum error of the equilateral triangular interpolation is 50.3% of the rectangular interpolation. In other words, for the same interpolation error and same order of interpolation, the right triangular interpolation needs smaller mesh size than the rectangular interpolation. The equilateral triangular interpolation

TABLE 7. Numerical maximum and RMS errors ratio, $\lambda/h = 20$.

Order	Max errors (◿/□)	Max errors (△/□)	RMS errors (◿/□)	RMS errors (△/□)
3	207%	100%	158.1%	71.4%
4	167%	50.3%	136.7%	54.4%

can use larger mesh size than the rectangular interpolation. If the RMS error in the interpolation is 10^{-4}, the number of sampling points per wavelength is about 12, 14, and 15 for the equilateral triangular, rectangular, and right triangular interpolations, respectively. If the error is decreased by a factor of 10, the sampling points should be increased only by 58.5%.

We describe how to find data points involved in the fourth order triangular interpolation for a given point. For the right triangular interpolations, find the three nearest data points to form a small equilateral triangle. Then extend to next 12 nearest data points to form a bigger right triangle. A similar approach is applied for the equilateral triangular interpolation. Table 7 lists the maximum and RMS errors ratio between triangular (◿/△) and rectangular (□) interpolations for the third and fourth order interpolations.

IV. APPLICATION OF DOUBLY PGF

The interpolation methods with the smallest interpolation errors from previous sections are applied to accelerate the evaluation of the doubly PGF. With the widely application of periodic structure, the efficient and accurate evaluation of periodic Green's functions is a fundamental problem in computational electromagnetics [12], [14]. Ewald transformation is one of the efficient and accurate methods to accelerate calculation PGF [12]. As given in [12], [19], a doubly PGF using Ewald method with a rectangular unit cell of periods a and b respectively along the x- and y-direction is

$$G(\mathbf{r},\mathbf{r}') = \sum_{m=-\infty}^{\infty}\sum_{n=-\infty}^{\infty} G_{mn}^{E} + \sum_{p=-\infty}^{\infty}\sum_{q=-\infty}^{\infty} \tilde{G}_{pq}^{E} \tag{7}$$

with

$$\begin{aligned} G_{mn}^{E} &= \frac{1}{2}\frac{e^{-j\mathbf{k}_{t00}\bullet\mathbf{r}_{mn}}}{4\pi R_{mn}} \\ &\quad\times\left[e^{-jkR_{mn}}\mathrm{erfc}\left(R_{mn}E - j\frac{k}{2E}\right)\right. \\ &\quad\left. + e^{jkR_{mn}}\mathrm{erfc}\left(R_{mn}E + j\frac{k}{2E}\right)\right] \\ \tilde{G}_{pq}^{E}(x,y) &= \frac{1}{2ab}\sum_{p=-\infty}^{\infty}\sum_{q=-\infty}^{\infty}\frac{\mathrm{erfc}\left(\gamma_{pq}/(2E)\right)}{\gamma_{pq}}e^{j(k_{xp}x+k_{yq}y)} \end{aligned} \tag{8}$$

where $\mathrm{erfc}(x)$ is the complementary error function, $\mathbf{k}_{t00} = k_x^{\mathrm{inc}}\hat{x} + k_y^{\mathrm{inc}}\hat{y}$, $\mathbf{r}_{mn} = ma\hat{x} + nb\hat{y}$, $k_{xp} = 2\pi p/a - k_x^{\mathrm{inc}}$, $k_{yq} = 2\pi q/b - k_y^{\mathrm{inc}}$, $\gamma_{pq} = \sqrt{k_{xp}^2 + k_{yq}^2 - k^2}$, $E = \sqrt{\pi/(ab)}$, and $R_{mn} = \sqrt{(x-ma)^2 + (y-nb)^2}$.

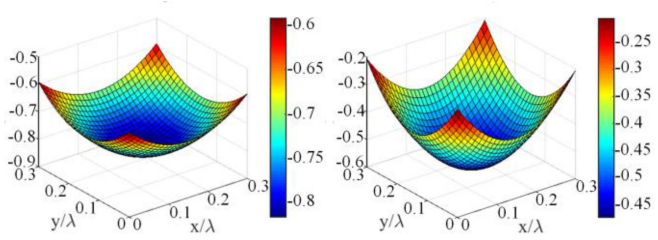

(a) Real part (b) Imaginary part

FIGURE 13. Regularized PGF in one period.

Before interpolating, the singularity of the PGF should be removed. The expression of regularization of the PGF is

$$G^{\mathrm{reg}} = \sum_{\mathbf{p}}^{\infty}\tilde{G}_{\mathbf{p}}^{E} + \sum_{\mathbf{n}}^{\infty}\left(G_{\mathbf{n}}^{E} - \delta_{\mathbf{n}}G_{\mathbf{n}}^{\infty}\right) \tag{9}$$

where $\mathbf{p} = (p,q)$, $\mathbf{n} = (m,n)$, $\delta_{\mathbf{n}} = \begin{cases} 1 & \mathbf{n} = (0,0),(1,0),(0,1),(1,1) \\ 0 & \text{otherwise} \end{cases}$, and $G_{\mathbf{n}}^{\infty}$ is the doubly PGF in free-space as

$$G_{mn}^{\infty} = \frac{e^{-jkR_{mn}}}{4\pi R_{mn}}e^{-j\mathbf{k}_{t00}\bullet\mathbf{r}_{mn}}. \tag{10}$$

When $m = 0$, $n = 0$ and $R = R_{00} = 0$, the asymptotic form of the PGF is obtained as

$$\begin{aligned} &\lim_{R\to 0}\left(\sum_{\pm}\frac{e^{\pm jkR}}{R}\mathrm{erfc}\left(RE \pm \frac{jk}{2E}\right) - \frac{2e^{-jkR}}{R}\right) \\ &= 2\left(jk\mathrm{erfc}\left(\frac{jk}{2E}\right) - \frac{2E}{\sqrt{\pi}}e^{\frac{k^2}{4E^2}}\right) + O\left(R^2\right) \end{aligned} \tag{11}$$

Using the periodicity of PGF, the asymptotic results of four corners can be obtained. Figures 13 (a) and (b) give the real and imaginary parts of the regularized PGF in one period, respectively. It is shown that the regularized PGF is smooth enough to be interpolated. Obviously, the function nearing the four corners changes more rapidly than others.

The relative interpolation error is defined as

$$R_g = \left|G^{\mathrm{reg}} - G^{\mathrm{reg}}_{\mathrm{interpolate}}\right| / \left|G^{\mathrm{reg}}\right| \tag{12}$$

The doubly PGF in a region of $a = 0.3\lambda$ by $b = 0.3\lambda$, total of 31 by 31 points, is interpolated from pre-calculated samples. The rectangular samples are 7 by 7 and the equilateral samples are 7 by 12 (more points along y-direction are needed because there is no periodicity in the samples). Figures 14, 15 and 16 show the relative interpolation error distributions for the third and fourth orders using the right triangular, equilateral triangular and rectangular interpolations, respectively. It is observed that although the equilateral triangular grids need more pre-calculated samples, the equilateral triangular interpolation has the smallest interpolation error for both $p = 3$ and $p = 4$, which confirms the earlier analysis and agrees with the lower order results. The right triangular interpolation has the largest relative interpolation error, while it uses 6 and 10 samples less comparing with the rectangular interpolation for the third and fourth orders, respectively.

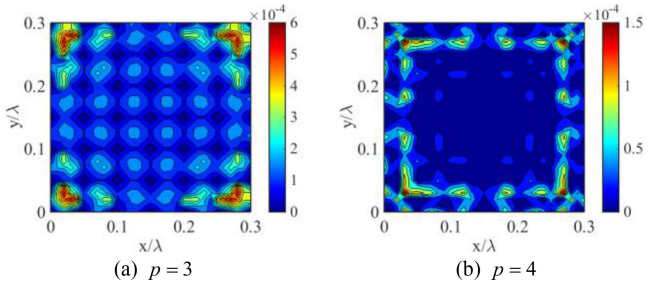

(a) $p = 3$ (b) $p = 4$

FIGURE 14. Relative interpolation errors of right triangular interpolation (◿).

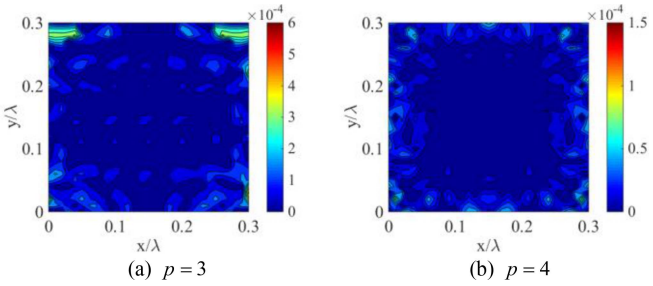

(a) $p = 3$ (b) $p = 4$

FIGURE 15. Relative interpolation errors of equilateral triangular interpolation (△).

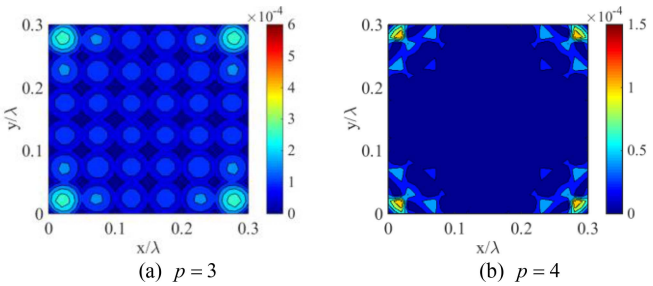

(a) $p = 3$ (b) $p = 4$

FIGURE 16. Relative interpolation errors of rectangular interpolation (□).

All the rectangular, right and equilateral triangular interpolations have the largest relative interpolation errors at the four corners of a period, where the doubly PGFs change faster.

Table 8 lists the interpolation CPU time running on a computer with Intel Core i7-4578U @3.00 GHz and 8 GB RAM. Calculating doubly PGF using Ewald method is still time-consuming. Here, 7 by 7 samples are calculated for the rectangular grids for both rectangular and right triangular interpolations, which take about 130 seconds. It takes 3161 seconds to calculate 31 by 31 points directly. Interpolation can reduce CPU time significantly in large scale problems. The third and fourth order right triangular interpolations are provided approximately 31.8% and 41.7% reduction in CPU time in the interpolations. The CPU time for the equilateral triangular interpolation is very close to the rectangular interpolation for both the third and fourth order interpolations, while it has the smallest interpolation error. Compared to the rectangular interpolations, the equilateral triangular interpolations need similar CPU time, while only 10 and 15 samples are required for the third and fourth order interpolations with the smallest interpolation errors.

TABLE 8. CPU time for the right triangular (◿), equilateral triangular (△) and rectangular interpolation (□).

-	Interpolation time	
Order	3	4
□	0.022s	0.036s
◿	0.015s	0.021s
△	0.022s	0.034s

V. CONCLUSION

In this article, both 1-D and 2-D interpolations are analyzed to minimize the interpolation errors. The interpolation areas in 2-D interpolation are chosen based on the smallest interpolation error for higher order right and equilateral triangular interpolations. Although the distance between two adjacent points of the equilateral triangular grid is $\sqrt{3}/2$ of the rectangular grid along the y-direction, the maximum and RMS errors of the fourth order equilateral triangular interpolation are only the half of the errors in the rectangular interpolation. Only $(p+1)(p+2)/2$ data points are used in the triangular interpolations. The asymptotic and numerical results of the rectangular, right and equilateral triangular interpolations can be used to estimate the interpolation error before interpolating. The appropriate interpolation method, order and grid size can be selected to optimize interpolation error and CPU time. In the higher order interpolations of the doubly PGF, the right triangular interpolation needs the least CPU time among three interpolation methods, while the equilateral triangular interpolation is the most accurate approach.

APPENDIX

A. 1-D INTERPOLATION

For the p'th order interpolation in 1-D, $p+1$ uniformly distributed sampling points are used to form a Lagrange interpolation polynomial as follows [17]:

$$L_p(x) = \sum_{i=-[p/2]}^{[(p+1)/2]} \left(J(x_i) \prod_{j=-[p/2], j\neq i}^{[(p+1)/2]} \frac{x - x_j}{x_i - x_j} \right) \tag{13}$$

where $x_i = ih$. The square brackets [] in the range of the summation and multiplication mean picking up the integer part. The range makes the central region between $-h/2$ and $h/2$ for even orders, and between 0 and h for odd orders. Therefore, the maximum error is at $x = h/2$ and

$$\begin{aligned} \left|R_p(x)\right|_{\text{Max}} &= \left|R_p(h/2)\right| \\ &= \frac{k^{p+1}}{(p+1)!} \left| \prod_{i=-[p/2]}^{[(p+1)/2]} \left(\frac{h}{2} - x_i \right) \right| \end{aligned} \tag{14}$$

After simplification, we have the asymptotic maximum error as shown in (1). The RMS error is given by

$$R_p^{\text{RMS}} = \sqrt{\frac{2}{h} \int_0^{h/2} dx \left|R_p(x)\right|^2}$$

$$= \frac{(kh)^{p+1}}{2^{p+1}(p+1)!}\sqrt{\int_0^1 dx \prod_{i=-[p/2]}^{[(p+1)/2]} (x-2i)^2}, \quad (15)$$

After performing the integral, we have the asymptotic form as shown in (2a) and (2b).

B. 2-D INTERPOLATION

In (3), when $p = q = 0$, we have

$$R_{0,0}(\alpha, x, y) = 2\sin|k(x\cos\alpha + y\sin\alpha)/2| \quad (16)$$

where $|x| \le h/2$, $|y| \le h/2$. The asymptotic form of the maximum error is derived as

$$R_{0,0}^{\text{Max}} \approx \frac{kh(|\sin\alpha| + |\cos\alpha|)}{2} = \frac{kh}{\sqrt{2}}\cos\left(\text{mod}\left(\alpha, \frac{\pi}{2}\right) - \frac{\pi}{4}\right) \quad (17)$$

It is a periodic function with a period of $\pi/2$. The RMS error has a form of

$$R_{0,0}^{\text{RMS}} = \sqrt{2}\sqrt{1 - \text{sinc}(kh\cos\alpha/2)\,\text{sinc}(kh\sin\alpha/2)} \approx \frac{kh}{2\sqrt{3}} \quad (18)$$

It is the same as 1-D result listed in Table 3. For non-zero orders,

$$R_{p,q}^{\text{Max}}(\alpha) \le \left|e^{-jkx\cos\alpha} - L_p(x)\right|_{\text{Max}} + \left|e^{-jky\sin\alpha} - L_q(y)\right|_{\text{Max}} = R_p^{\text{Max}}(kh|\cos\alpha|) + R_q^{\text{Max}}(kh|\sin\alpha|) \quad (19)$$

If $p = q$, the above equation is simplified to (5).

For the RMS error, we have

$$\left|e^{-jk(x\cos\alpha+y\sin\alpha)} - L_p(x)L_q(y)\right|^2 = \left|R_p(x)\right|^2 + \left|R_q(y)\right|^2 + 2\text{Re}\left[R_p(x)L_p^*(x)e^{-jky\sin\alpha}R_q^*(y)\right] \quad (20)$$

The leading term of the third term is $2R_p(x)R_q^*(y)$. The integrals over x and y yield the average of the error. The RMS error is derived as

$$R_{p,p}^{\text{RMS}} \approx R_p^{\text{RMS}}(kh)\sqrt{\cos^{2(p+1)}\alpha + \sin^{2(p+1)}\alpha} \quad (21a)$$

for even p, and

$$R_{p,p}^{\text{RMS}} \approx R_p^{\text{RMS}}(kh) \times \sqrt{\left(\cos^{p+1}\alpha + \sin^{p+1}\alpha\right)^2 - \frac{c\sin^{p+1}(2\alpha)}{2^p}} \quad (21b)$$

for odd $p = 2m - 1$, where

$$c = 1 - \frac{\left[\int_0^1 dx\, x(x-2m)\prod_{i=1}^{m=1}\left(x^2 - 4i^2\right)\right]^2}{\int_0^1 dx x^2(x-2m)^2\prod_{i=1}^{m=1}\left(x^2-4i^2\right)^2}.$$

It is found that for $p = 1$, $c = 1/6$, and for $p = 3$, $c = 183/1030$. The plots of $p = 1, 2$ show excellent agreements between the numerical results and the above expressions [14]. For the higher orders, by ignoring the second term inside the square root of (21b), we can simplify (21a) and (21b) into (6).

REFERENCES

[1] J. M. Song and W. C. Chew, "Multilevel fast multipole algorithm for combined field integral equation of electromagnetic scattering," *Micro. Opt. Tech. Lett.*, vol. 10, no. 1, pp. 14–19, Sep. 1995.

[2] R. D. Graglia, D. R. Wilton, and A. F. Peterson, "Higher order interpolatory vector bases for computational electromagnetics," *IEEE Trans. Antennas Propag.*, vol. 45, no. 3, pp. 329–342, Mar. 1997.

[3] *Fast and Efficient Algorithms in Computational Electromagnetics*, W. C. Chew, J.-M. Jin, E. Michielssen, and J. M. Song, Eds. London, U.K.: Artech House, 2001.

[4] J. M. Jin, *The Finite Element Method in Electromagnetics*, 2nd ed. New York, NY, USA: Wiley, 2002.

[5] G. Kang, J. M. Song, W. C. Chew, K. C. Donepudi, and J. M. Jin, "A novel grid-robust higher-order vector basis function for the method of moments," *IEEE Trans. Antennas Propag.*, vol. 49, no. 6, pp. 908–915, Jun. 2001.

[6] K. Yasumoto and K. Yoshitomi, "Efficient calculation of lattice sums for free-space periodic Green's function," *IEEE Trans. Antennas Propag.*, vol. 47, no. 6, pp. 1050–1055, Jun. 1999.

[7] C. Craeye and F. Capolino, "Accelerated computation of the free space Green's function of semi-infinite phased arrays of dipoles," *IEEE Trans. Antennas Propag.*, vol. 54, no. 3, pp. 1037–1040, Mar. 2006.

[8] K. A. Michalski and J. R. Mosig, "Multilayered media Green's functions in integral equation formulations," *IEEE Trans. Antennas Propag.*, vol. 45, no. 3, pp. 508–519, Mar. 1997.

[9] G. S. Mário and A. F. Carlos, "A new acceleration technique with exponential convergence rate to evaluate periodic green functions," *IEEE Trans. Antennas Propag.*, vol. 53, no. 1, pp. 347–355, Jan. 2005.

[10] G. Valerio, P. Baccarelli, P. Burghignoli, and A. Galli, "Comparative analysis of acceleration techniques for 2-D and 3-D Green's functions in periodic structures along one and two directions," *IEEE Trans. Antennas Propag.*, vol. 55, no. 6, pp. 1630–1643, Jun. 2007.

[11] K. Chen, J. M. Song, and T. Kamgaing, "Accurate and efficient computation of layered medium doubly periodic Green's function in matrix-friendly formulation," *IEEE Trans. Antennas Propag.*, vol. 63, no. 2, pp. 809–814, Feb. 2015.

[12] F. T. Celepcikay, D. R. Wilton, D. R. Jackson, and W. A. Johnson, "Interpolation of ewald-accelerated periodic green's function representations for homogeneous or layered media," *IEEE Trans. Antennas Propag.*, vol. 65, no. 5, pp. 2517–2525, May 2017.

[13] H. F. Yang and A. E. Yilmaz, "A log-scale interpolation method for layered medium Green's functions," in *Proc. IEEE Int. Symp. Antennas Propag. USNC/URSI Nat. Radio Sci. Meeting*, Boston, MA, USA, Jul. 2018, pp. 2495–2496.

[14] W. Luo, J. B. Liu, Z. R. Li, and J. M. Song, "Efficient triangular interpolation methods: Error analysis and applications," *IEEE Antennas Wireless Propag. Lett.*, vol. 19, no. 6, pp. 1032–1036, Jun. 2020.

[15] J. M. Song and W. C. Chew, "Interpolation of translation matrix in MLFMA," *Micro. Opt. Tech. Lett.*, vol. 30, no. 2, pp. 109–114, Jul. 2001.

[16] O. M. Bucci, C. Gennareli, and C. Savarese, "Optimal interpolation of radiated fields over a sphere," *IEEE Trans. Antennas Propag.*, vol. 39, no. 2, pp. 1633–1643, Nov. 1991.

[17] M. Abramowitz and I. A. Stegun, *Handbook of Mathematical Functions*. New York, NY, USA: Dover, 1972.

[18] W. H. Press, S. A. Teukolsky, W. T. Vetterling, and B. P. Flannery, *Numerical Recipes*, 2nd ed. New York, NY, USA: Cambridge Univ. Press, 1992.

[19] A. F. Peterson, S. L. Ray, and R. Mittra, *Computational Methods for Electromagnetics*. Oxford, U.K.: Oxford Univ. Press, 1998.